Structuring a Quantum Solvent around a Weakly Bound Dopant: The He–CS2((3)Sigma u) Complex

6 AUTHORS, INCLUDING:

Gerardo Delgado-Barrio
Spanish National Research Council
246 PUBLICATIONS   **2,961** CITATIONS

Pablo Villarreal
Spanish National Research Council
202 PUBLICATIONS   **2,617** CITATIONS

Ersin Yurtsever
Koc University
138 PUBLICATIONS   **1,230** CITATIONS

Franco A Gianturco
Sapienza University of Rome
448 PUBLICATIONS   **6,225** CITATIONS

Structuring a Quantum Solvent around a Weakly Bound Dopant: The He−Cs₂(³Σᵤ) Complex[†]

Rita Prosmiti, Gerardo Delgado-Barrio, and Pablo Villarreal*

Instituto de Física Fundamental, C.S.I.C., Serrano 123, 28006 Madrid, Spain

Ersin Yurtsever

Department of Chemistry, Koç University, Rumeligeneri Yolu, 34450 Sariyer, Istanbul, Turkey

Emanuele Coccia and Franco A. Gianturco

Department of Chemistry and CNISM, University of Rome La Sapienza, Piazzale A. Moro 5, 00185 Rome, Italy

The structure and energetics of ^{3,4}HeCs$_2$($^3\Sigma_u$) molecules are analyzed from first principles. Fixing the cesium dimer at its equilibrium distance, the electronic structure was determined through ab initio methods at the CCSD(T) level of theory using a large basis set to compute the interaction energies. At the T-shaped geometry, there is a shallow well with a depth of ∼2 cm^{-1} placed at R ∼6.75 Å, R being the distance from the center of mass of Cs$_2$ to He. That depth gradually decreases to ∼0.75 cm^{-1}, while R increases to about 11.5 Å at linear arrangements. A simple model of adding atom−atom Lennard-Jones potentials with well-depth and equilibrium distance parameters depending on the angular orientation was found to accurately reproduce the ab initio points. Using this analytical form, variational calculations at zero total angular momentum are performed, predicting a single bound level at ∼−0.106 (∼−0.042) cm^{-1} for the boson (fermion) species. Further calculations using Quantum Monte Carlo methods are carried out and found to be in good agreement with the variational ones. On the basis of the present results, such analytical expression could in turn be used to describe the structure and binding of larger complexes and therefore opens the possibility to further studies involving such aggregates.

I. Introduction

There has been a truly remarkable progress and fast development of a broad variety of methods for producing, trapping, and controlling atoms in the gas phase, based on techniques involving laser and evaporative cooling of the samples. The rapid implementation of ever more sophisticated devices for manipulating and studying ultracold matter using optical and electromagnetic fields is currently expanding the interest of such experiments into areas like condensed matter physics[1] and quantum information processes.[2]

The successes achieved with mainly alkali metal atoms have spurred in turn major efforts to extend the findings of ultracold physics into the realm of molecules for which, however, laser cooling schemes are not straightforwardly applicable. Hence, the additional stride into the realm of producing cold and ultracold molecules and the desire to discover what these advances have to offer for our understanding of chemical processes.[3−5]

Perhaps one the most general ways for cooling molecules has been to simply immerse them in a very-low-T bath of a suitable buffer gas, thereby relying on the ensuing elastic collisions to dissipate the excess molecular energies. This method has been pioneered by Doyle and co-workers[6] and also implemented by Bakker et al.[7] and, although simple in principle, provides a number of challenges associated with such experi-

ments.[8] On the other hand, since one of the most common species used for this type of cooling has been helium, then it becomes of importance to be able to know as realistically as possible the details of the interaction forces between the sample molecule and the ^{4}He or ^{3}He partners.[9,10] These molecules, in fact, must thermalize to the temperature of the buffer gas before reaching the wall of the chamber, a feat that requires several hundred collisions and therefore needs some reliable knowledge of the relevant He-molecule cross sections at low temperatures to guide the experimental planning.

Along a different route to producing cold molecules, one successful variety has been to start from ultracold ensembles of alkali metal atoms that can be produced through laser cooling and then by pairing the cold atoms together through either photoassociation or by magnetic Feshbach resonance tuning.[11] In both cases, very low collision energies can be reached (<μK), thereby producing molecules with little rotational excitation but into highly excited vibrational states.[12]

It should have become clear from the above discussion that the production of alkali metal molecules, either homonuclear or heteronuclear species, and their further manipulation within collisional regimes (and indeed using initially a weakly interacting gas like helium) also requires information on the interaction forces at play and knowledge of the likely structures which could be formed by such systems at low (from 1 K to 1 mK) and ultralow (<1 μK) temperatures. The aim of the present paper is therefore that of investigating the interaction between a well-studied alkali metal dimer that can be formed by photoassociation, the Cs$_2$ molecule in its $^3\Sigma_u$ electronic state and one

Structuring a Quantum Solvent around a Weakly Bound Dopant

J. Phys. Chem. A, Vol. 113, No. 52, 2009 **14719**

TABLE I: Equilibrium Distance, r_{eq}, and Well-Depth, D_e, Values Obtained through the Use of Different ECPs for the Cesium Dimer[a]

this work	r_{eq} (Å)	D_e (cm^{-1})
LANL2DZ[17]	7.5	132.08
Hay−Wadt[18]	8.1	237.69
ECP46MWB[19]	7.8	91.38
ECP46MDF[20]	6.5	229.61
CRENBL[21]	6.8	211.68
Expt. Xie et al.[22]	6.235	279.349
Foucrault et al.[23]	6.355	233
	6.31	267
Li et al.[24]	6.30	295

[a] Earlier reported values of these magnitudes are also included.

representative ^{4}He or ^{3}He atom, to analyze the possible bound structures that are likely to exist for such a weakly interacting system. The present study is also meant to help shed some light on the possible behavior of Cs_2 as a dopant for superfluid He droplets, a further low-T situation with broad chemical implications[13−15] that, as important prerequisite, requires some knowledge of the initial structure of the smallest triatomic complex. In this context, visible absorption spectra of cesium-doped cold helium nanodroplets involving the triplet ground state have been recently reported.[16]

The following section (Section II) analyses the detailed features of the relevant potential energy surface (PES) while Section III discusses the methods to calculate its bound states. Section IV presents the results obtained, and the conclusions are given by Section V.

II. The Interaction Potential

A. Ab Initio Electronic Structure Computations. All ab initio calculations are performed with the Gaussian03 program,[17] using the spin restricted single and double excitations coupled cluster method with perturbative triples [RCCSD(T)] correlating only the valence electrons. We use Jacobi coordinates (r, R, θ) to describe the potential surface of $HeCs_2$ complex, where R is the intermolecular distance of He atom from the center of mass of Cs_2, r is the bond length of Cs_2, here fixed at its equilibrium value $r_{eq} = 6.8$ Å, and θ is the angle between the $\boldsymbol{R}$ and $\boldsymbol{r}$ vectors.

Angles are incremented by 10° from 0 to 90° and distances extended out to 24 Å, using different spacings between R values depending on its orientation. The total number of computed points was 355. To assess the quality of the calculations, different choices of basis set expansions were implemented and tested before carrying out the final calculations. For instance, the potential curve of the Cs_2 molecular partner was generated by selecting five effective core potentials (ECP) from different groups within the CCSD(T) approach: the LANL2DZ,[17] which uses 52 primitive GTOs contracted to 24; the Hay-Wadt[18] and the ECP46MWB,[19] which use 46 and 50 primitive GTOs contracted to 16 and 34, respectively; the ECP46MDF,[20] which uses 270 primitive functions contracted to 192; and the CRENBL[21] effective core potential, which uses 88 primitive GTOs contracted to 80. In Table I, we present the values of r_{eq}, and D_e well-depth, obtained using the above-mentioned ECPs, together with previous estimations of those magnitudes. The most recent reported potential energy curve, derived from fluorescence measurements,[22] presents values of 6.235 Å and 279.349 cm^{-1}, in accordance with some earlier theoretical estimations.[23,24] In our calculations, accurate results are obtained with the use of ECP46MDF. However, CRENBL turned out to

produce a realistic description of the dimer triplet potential curve (6.8 Å, and 211.683 cm^{-1}), while keeping the computational effort within acceptable limits. In fact, the latter values are in line with some other estimates on this system, as 6.35 Å and 233 cm$^{-1\,23}$ (see Table 7 in that reference). We should note that CRENBL already includes 5s and 5p electrons in the definition of the valence space allowing an explicit treatment of core−valence electron correlation in subsequent calculations. Keeping this requirement, the particular ECP choice to describe the dimer is expected to be of minor significance on the He−Cs_2 interaction, although slightly deeper wells could be obtained if pseudopotentials like ECP46MDF were considered. Thus, final calculations were carried out within the CRENBL choice of the ECP for the Cs dimer. The basis set for the He atom was also varied from cc-pVQZ to cc-pV5Z, to aug-cc-pV5Z, and then to d-aug-cc-pVQZ and d-aug-cc-pV5Z. In this way, the interaction energies using the supermolecular approach, $\Delta E = E_{HeCs_2} - E_{He}^{BSSE} - E_{Cs_2}^{BSSE}$, were obtained. The best choice, including the BSSE correction,[25] turned out to be the d-aug-cc-pVQZ in terms of strength of the very weak interaction and feasibility of computational times, producing variations of the minimum values of the attractive wells that essentially are coincident with those given by the d-aug-cc-pV5Z choice. For the two limiting orientations of He with respect to the cesium dimer, that is, collinear and perpendicular, we present the dependence of the interaction energies as a function of the R distance with the basis set in Tables II and III, respectively. As above-mentioned, the use of d-aug-cc-pV5Z slightly improves the quality obtaining lower interaction energies with respect to d-aug-cc-pVQZ. It results, however, too expensive for an exhaustive search.

B. Analytical Representation of the Potential Surface. To represent the potential energy surface for the $HeCs_2$ complex, we used an analytical functional form to fit the CCSD(T) ab initio points. One common method starts by considering an expansion in Legendre polynomials, $P_\lambda(\cos \theta)$; thus for He−Cs_2 we have

$$V(R, \theta) = \sum_{\lambda=0}^{\lambda_{max}} V_\lambda(R) P_\lambda(\cos \theta) \tag{1}$$

with $\lambda = $ even ($\lambda_{max} = 18$) due to the symmetry of the system with respect to $\theta = \pi/2$, using all $N_\theta = 10$ angles to achieve convergence. After performing some suitable fit to each $V(R, \theta_k)$, $k = 1, N_\theta$, one obtains the $V_\lambda(R)$ by solving at each R value the system of linear equations

$$V(R, \theta_k) = \sum_{\lambda=0}^{18} V_\lambda(R) P_\lambda(\cos \theta_k), \quad k = 1, N_\theta \tag{2}$$

which involves an initial calculation of the inverse matrix of Legendre polynomials $\underline{\underline{P}}^{-1}$, with $P_{k\lambda} = P_\lambda(\cos \theta_k)$. This constitutes the so-called collocation procedure and is being currently used for fitting He-dimer PESs.[26] However, this method leads sometimes to undesired results. In particular, for the system under study that presents weak interaction and large anisotropy, one finds that the $V_\lambda(R)$ functions exhibit large oscillations in regions where one expects that the nuclear wave functions usually start having an important role. Indeed, this procedure guarantees the continuity of the interaction along the R variable for each orientation, but the reciprocal is not true; at each fixed R, the function along θ

TABLE II: Dependence on the Basis Set Used for the He Atom of Interaction Energies, ΔE (See Text), at the Collinear Arrangement of He−Cs$_2$

	ΔE (cm^{-1})					
R (Å)	QZ	5Z	aug-QZ	aug-5Z	d-aug-QZ	d-aug-5Z
6.00	2327.771	2282.105	2198.207	2173.477	2179.948	2144.296
6.50	952.525	930.859	883.128	877.674	877.092	868.297
7.00	523.800	510.103	472.358	469.742	468.505	467.147
7.50	293.591	284.553	256.521	254.344	251.328	251.031
8.00	155.384	149.515	131.222	129.670	126.016	125.660
8.50	77.383	73.710	62.534	61.598	58.731	58.413
9.00	36.467	34.253	27.632	27.100	25.235	25.033
9.50	16.246	14.946	11.101	10.805	9.663	9.549
10.00	6.740	5.982	3.781	3.619	2.935	2.871
10.50	2.487	2.042	0.789	0.701	0.297	0.261
11.00	0.692	0.425	−0.296	−0.341	−0.575	−0.595
11.20	0.329	0.108	−0.472	−0.506	−0.692	−0.709
11.40	0.087	−0.097	−0.567	−0.593	−0.740	−0.753
11.50	−0.071	−0.168	−0.607	−0.615	−0.743	−0.758
11.60	−0.170	−0.224	−0.612	−0.626	−0.717	−0.753
11.80	−0.227	−0.297	−0.594	−0.626	−0.675	−0.724
12.50	−0.266	−0.338	−0.504	−0.509	−0.545	−0.548
13.00	−0.240	−0.290	−0.401	−0.402	−0.421	−0.421
13.50	−0.197	−0.233	−0.311	−0.310	−0.320	−0.320
14.00	−0.156	−0.182	−0.238	−0.238	−0.242	−0.242
15.00	−0.095	−0.110	−0.141	−0.141	−0.141	−0.140
16.00	−0.058	−0.067	−0.086	−0.085	−0.085	−0.084
17.00	−0.037	−0.043	−0.054	−0.054	−0.053	−0.052
18.00	−0.024	−0.028	−0.035	−0.035	−0.034	−0.033
20.00	−0.011	−0.013	−0.016	−0.015	−0.015	−0.014
22.00	−0.006	−0.007	−0.008	−0.007	−0.007	−0.006
24.00	−0.003	−0.003	−0.004	−0.003	−0.003	−0.002

TABLE III: Same as Table II for the perpendicular Orientation of He−Cs$_2$

	ΔE (cm^{-1})					
R (Å)	QZ	5Z	aug-QZ	aug-5Z	d-aug-QZ	d-aug-5Z
0.00	1569.697	1542.587	1485.339	1480.392	1485.508	1479.274
1.00	1289.866	1264.752	1207.830	1203.493	1207.395	1204.355
2.00	749.114	729.726	678.450	673.994	672.051	671.302
3.00	319.697	307.866	274.717	271.238	263.962	263.206
4.00	101.085	95.426	79.843	78.240	72.854	72.264
5.00	23.317	21.084	15.094	14.528	12.197	11.941
6.00	3.042	2.208	0.144	−0.035	−0.874	−0.964
6.50	0.342	−0.182	−1.400	−1.497	−1.985	−2.037
7.00	−0.615	−0.956	−1.698	−1.749	−2.028	−2.057
7.25	−0.777	−1.055	−1.648	−1.683	−1.890	−1.912
7.50	−0.830	−1.059	−1.536	−1.561	−1.715	−1.731
7.75	−0.817	−1.007	−1.397	−1.414	−1.528	−1.539
8.00	−0.769	−0.927	−1.250	−1.262	−1.345	−1.353
8.50	−0.632	−0.745	−0.972	−0.977	−1.020	−1.024
9.00	−0.495	−0.576	−0.741	−0.743	−0.765	−0.766
9.50	−0.379	−0.440	−0.562	−0.562	−0.574	−0.573
10.00	−0.290	−0.335	−0.427	−0.427	−0.432	−0.431
12.00	−0.104	−0.120	−0.153	−0.152	−0.152	−0.151
14.00	−0.043	−0.049	−0.062	−0.062	−0.061	−0.060
16.00	−0.020	−0.022	−0.028	−0.028	−0.027	−0.026
18.00	−0.010	−0.011	−0.014	−0.013	−0.013	−0.012
20.00	−0.005	−0.006	−0.007	−0.006	−0.006	−0.005
22.00	−0.003	−0.003	−0.004	−0.003	−0.003	−0.002
24.00	−0.002	−0.002	−0.002	−0.001	−0.001	0.000

may not be smooth enough. Hence, we decided to perform a pure analytical fit within a small region of energy (below 5 cm^{-1}) in the two coordinates (R, θ) by assuming that the potential could be given by the addition of two angle-dependent He−Cs interactions, each of them described by a Lennard-Jones function

$$V(x) = d[(\bar{x}/x)^{12} - 2(\bar{x}/x)^6] \quad (3)$$

where d is the well-depth and $\bar{x}$ is the equilibrium distance. At $\theta = 0$, one realizes that such an addition chiefly reduces to the interaction of He with the nearest Cs atom. A cubic spline fitting to the ab initio points presents a minimum of -0.7461 cm^{-1} at $R = 11.5116$ Å; the nearest Cs atom is here at a distance of $11.5 - 0.5 \times r_{eq} = 8.1$ Å. Fixing then the equilibrium parameter $\bar{x}$ at 8.1 Å, the fit produces a slightly lower value of $d = 0.7$ cm^{-1}. For the perpendicular orientation, the fit to the ab initio points presents a minimum of -2.0822 cm^{-1} at $R = 6.7488$ Å.
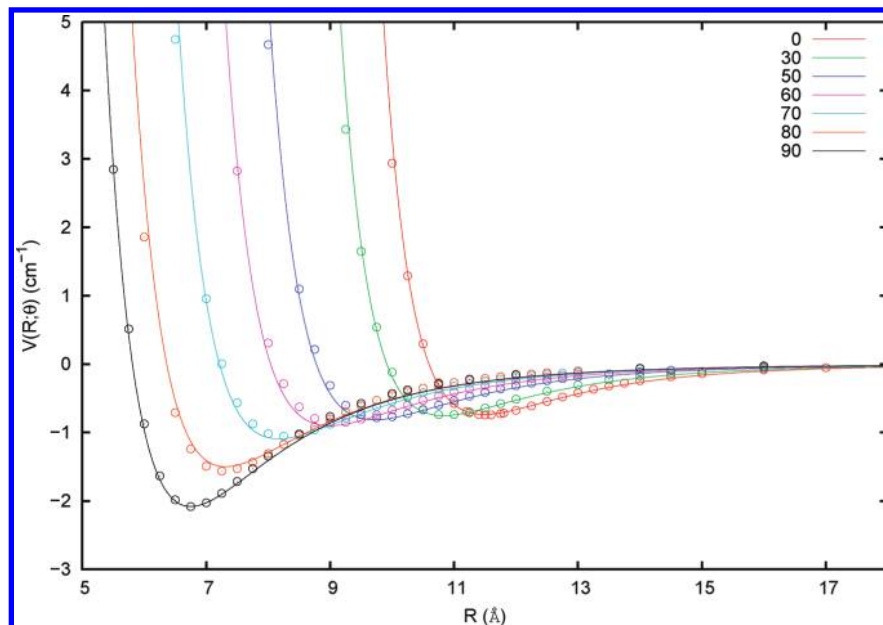
Figure 1. Computed ab initio points (circles) and analytical fits (solid lines), as functions of the relative distance R, at the indicated orientations of the He atom respect to the Cs_2 molecular axis.

Hence, using simple geometrical arguments one arrives at the values of $d = 2.0822/2 = 1.0411$ cm^{-1} and $\bar{x} = 7.5685$ Å. We then assume a simple dependence of the parameters on the orientation angle, namely

$$d(\theta) = 0.7 + 0.3411 \times f(\theta)$$
$$\bar{x}(\theta) = 8.1 - 0.5341 \times g(\theta) \quad (4)$$

which reproduces the values of d and $\bar{x}$ at $\theta = 0$, and $\pi/2$ as long as the $f(\theta)$, $g(\theta)$ sloping functions fulfill the conditions

$$f(0) = g(0) = 0$$
$$f(\pi/2) = g(\pi/2) = 1 \quad (5)$$

Simple inspection of the different angular curves reveals that there is a slower variation of them when increasing θ from the linear arrangement than when one approaches the latter from the perpendicular orientation, the behavior being more marked for the well depths than for the equilibrium values. This suggests for the f and g functions the use of some power of $(1 - \cos \theta)$. In the end, in the interval $0 \leq \theta \leq \pi/2$, we found suitable to use

$$f(\theta) = f(\theta) = (1 - \cos \theta)^4$$
$$g(\theta) = g(\theta) = (1 - \cos \theta)^2 \quad (6)$$

for energies below 5 cm^{-1} and assume a symmetric behavior in $\pi/2 \leq \theta \leq \pi$. In practice, this is equivalent to replacing $\cos \theta$ in eq 6 by its absolute value. Figure 1 depicts the $V(R, \theta)$ analytical functions obtained using the procedure outlined above, together with the ab initio data, for $\theta = 0, 30, 50, 60, 70, 80$, and $90°$; taking into account the simplicity of the model proposed, the agreement is really good. In fact, the total averaged standard deviation is of $\sigma = 0.027$ cm^{-1} in the energy range considered, which is assumed to be of major importance in the calculation of bound states. Larger deviations are found at higher energies, where the addition of pairwise Lennard-Jones potentials clearly becomes inadequate. A more adequate description

TABLE IV: Interaction Energies, ΔE (See Text) and Analytical Potential $V(R, \theta)$ Values Together with Their Deviations[a]

(θ, R)	ΔE	$V(\theta, R)$	$\Delta E - V$	σ_θ
(0,11.50)	−0.746	−0.7357	−0.010	0.012
(10,11.40)	−0.744	−0.7374	−0.007	0.012
(20,11.25)	−0.742	−0.7414	−0.0006	0.014
(30,10.75)	−0.738	−0.7515	0.013	0.020
(40,10.50)	−0.750	−0.7645	0.014	0.024
(50,9.75)	−0.783	−0.8145	0.031	0.027
(60,9.00)	−0.854	−0.9011	0.047	0.033
(70,8.25)	−1.054	−1.0888	0.035	0.030
(80,7.25)	−1.564	−1.4975	0.067	0.040
(90,6.75)	−2.082	−2.0822	0.0002	0.044

[a] Energies are in cm^{-1}, angles in degrees, and distances in Å. σ_θ is the partial average standard deviation for each θ.
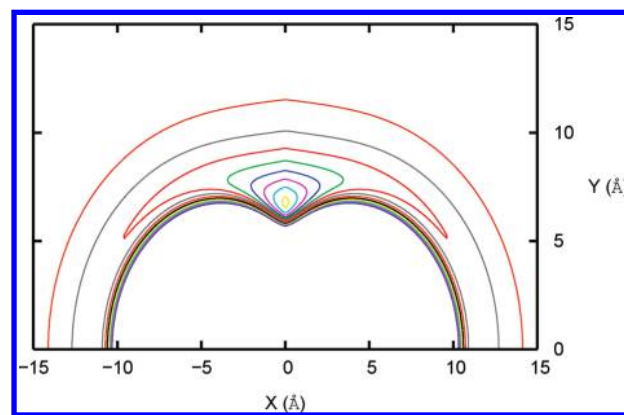

Figure 2. Contour plot of the analytical PES in terms of $X = R \cos \theta$ and $Y = R \sin \theta$. Starting from -2 cm^{-1}, isolines are plotted at intervals of 0.25 cm^{-1}.

of the short-range region would be obtained by using a modified, improved version of the Lennard-Jones functional form.[27] In Table IV, we list the deviations obtained at the minimun energy ab initio point for each θ, as well as the partial averaged standard deviation, σ_θ, for each angular value. Figure 2 shows a contour plot of the analytical surface in terms of $(R \cos \theta, R \sin \theta)$ to give a pictorial view of the very marked shallowness of the

14722   *J. Phys. Chem. A, Vol. 113, No. 52, 2009*

Prosmiti et al.

TABLE V: Parameters of the Extrapolations at Short and Long Distances Performed on the ab Initio Data at the 10 Orientations Indicated

$\theta°$	A (cm^{-1})	α (Å^{-1})	B (cm^{-1} Å$^{\beta}$)	β
0	278137788.4551	1.6608	11457505596.3635	9.1066
10	55009414.4514	1.4339	884619288.9493	8.2934
20	64172089.7800	1.5542	873499408.8709	8.3121
30	4674391.1918	1.2455	112126116.4231	7.6636
40	150801.1967	0.7522	552146980.8035	8.2443
50	20104.3601	0.4721	869999220.3332	8.4562
60	2944.3097	0.0881	459122135.2401	8.2930
70			427528983.9724	8.3151
80			1120216686.4785	8.6731
90			607750454.5666	8.4789

present interaction; isolines are from -2 cm^{-1} at intervals of 0.25 cm^{-1}. Note that at cos $\theta = 0$ the surface, although continuous, is no longer derivable. This would constitute a serious drawback for carrying out calculations involving derivatives of the potential, as classical trajectories, but does not imply any trouble in the present quantum scenario.

As mentioned above, one of the goals of the present fit is to avoid undesired oscillations in the coefficients $V_\lambda(R)$ of the expansion of $V(R, \theta)$ in Legendre polynomials. To stress this issue, at the 10 values of θ the ab initio points were further adjusted using a cubic spline interpolation. For $\theta \leq 60°$ an extrapolation at short distances, where ab initio energies become huge and positive, was done using a Born–Mayer form ($Ae^{-\alpha R}/R$). Additionally, at each orientation, a further ($-B/R^{\beta}$) term was added to describe large distances. The corresponding parameters are listed in Table V. In Figure 3a, we plot the coefficients obtained after collocation; from $\lambda = 6$, they show remarkable oscillations that should affect further calculations. In contrast, the coefficients shown in Figure 3b, coming from the analytical fit, exhibit as expected a completely regular
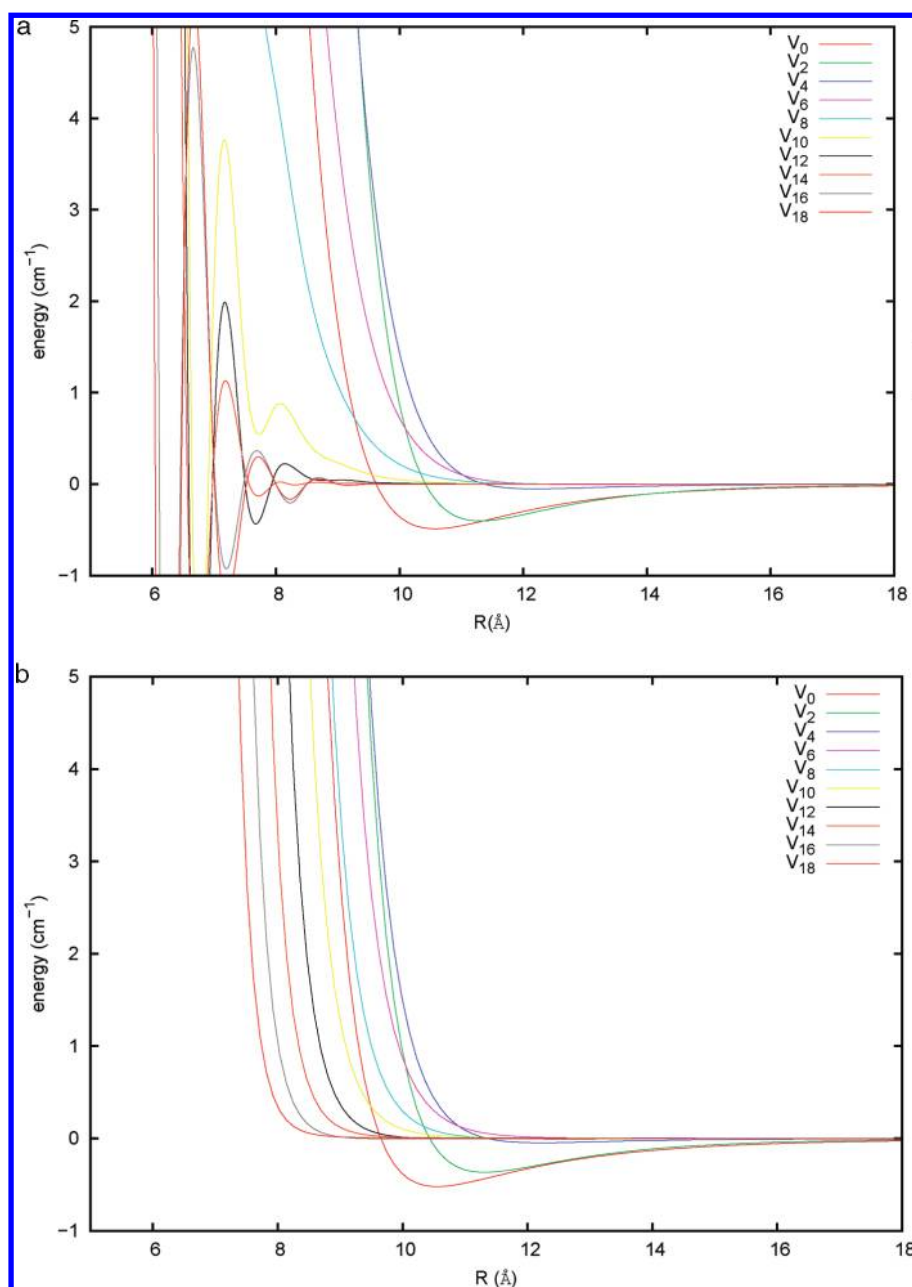

Figure 3. $V_\lambda(R)$ coefficients of the expansion of eq 1 coming from (a) the numerical fit to the 10 θ values of ab initio data and (b) the analytical fit.

behavior. The ab initio data, as well as the full, final PES is available on request from the authors.

III. Bound State Calculations

A. Variational Method. Considering the cesium dimer as a pseudo$-^1\Sigma$ partner,[28] that is, ignoring spin effects for the moment, the rovibrational Hamiltonian in the Jacobi coordinate system has the form[29,30]

$$\hat{H} = -\frac{\hbar^2}{2\mu}\frac{\partial^2}{\partial R^2} + B_e\hat{j}^2 + \frac{\hat{l}^2}{2\mu R^2} + V(R,\theta) \qquad (7)$$

where $B_e = 1/mr_{eq}^2$ is the rotational constant associated to the diatom frozen at its equilibrium distance r_{eq}, m being the atomic mass of cesium. $\mu = 2m_{He}m/(m_{He} + 2m)$ is the He$-$Cs$_2$ reduced mass. $V(R,\theta)$ describes the helium$-$cesium rotor interaction, while $\hat{l}$ and $\hat{j}$ are the angular momentum operators associated with the vectors R and r, respectively, leading to a total angular momentum $\hat{J} = \hat{l} + \hat{j}$. More correctly, we should replace in eq 7 the total diatomic angular momentum $\hat{j}$ by the nuclear diatomic rotational angular momentum which, since the electronic $^3\Sigma_u$ state of alkali dimer molecules corresponds[31] to a Hund's case (b),[32,33] reduces to $\hat{N} = \hat{j} - \hat{S}$, $\hat{S}$ being the electronic spin operator. Additionally, we should also incorporate the spin coupling effects (spin$-$spin and spin$-$rotation) in the more complete Hamiltonian. This extension will be considered in future work, while we limit the present analysis to the simplified Hamiltonian of eq 7 or to account for only diagonal terms of the $\hat{N}^2$ operator. Given the smallness of the additional coupling terms, however, we do not expect any major effect on the present conclusions.

A body-fixed (BF) frame, with the Z^{BF} axis parallel to the vector $\hat{R}$ is used. We consider basis functions of the form

$$\Psi_{nj\Omega}^{JM}(R,\hat{r}) = f_n(R)\mathscr{W}_{j\Omega}^{JM}(\hat{R},\hat{r}) \qquad (8)$$

Here, f_n are radial functions associated with the He$-$Cs$_2$ stretching motion which will be specified later on. In eq 8, the angular functions $\mathscr{W}_{j\Omega}^{JM}$ depend on the orientation of $\hat{R} \equiv (\theta_R, \phi_R)$ with respect to a space-fixed (SF) reference system, and on the orientation $\hat{r} \equiv (\theta, \phi)$ in the BF frame. They are expressed as[34]

$$\mathscr{W}_{j\Omega}^{JM}(\hat{R},\hat{r}) = \sqrt{\frac{2J+1}{4\pi}}\mathscr{D}_{M\Omega}^{J*}(\phi_R,\theta_R,0)Y_{j\Omega}(\theta,\phi) \quad (9)$$

where $\mathscr{D}_{M\Omega}^{J}$ are Wigner rotation matrices labeled by J, the quantum number associated with the total angular momentum $\mathbf{J}$, and by M and Ω, the quantum numbers associated with the projections of $\mathbf{J}$ on Z^{SF} and Z^{BF}, respectively, and $Y_{j\Omega}$ are spherical harmonics. The relevant symmetry operators of the system are those corresponding to the total inversion ε^* and the exchange of cesium nuclei $\mathscr{P}$. The basis functions eq 9 are already eigenfunctions of $\mathscr{P}$ with eigenvalue $\eta = (-1)^j$, and the action of the total inversion over them is

$$\varepsilon^*[\mathscr{W}_{j\Omega}^{JM}] = (-1)^J\mathscr{W}_{j-\Omega}^{JM} \qquad (10)$$

Hence, a symmetry-adapted basis set is defined as

$$\Psi_{nj\Omega}^{JM\epsilon\eta}(R,\hat{r}) = f_n(R)\Theta_{j\Omega}^{JM\epsilon\eta}(R,\hat{r}) \qquad (11)$$

which is eigenfunction of $\mathscr{E}^*$ with eigenvalue ϵ, and where

$$\Theta_{j\Omega}^{JM\epsilon\eta} = [2(1 + \delta_{\Omega 0})]^{-1/2}\{\mathscr{W}_{j\Omega}^{JM} + \epsilon(-1)^J\mathscr{W}_{j-\Omega}^{JM}\} \qquad (12)$$

The radial $f_n(R)$ functions appearing in eq 8 are numerically obtained as follows:[35] at different fixed orientations θ_n, $n = 1, N$, one looks for just the ground energy level of the Schrödinger equation

$$\left[-\frac{\hbar^2}{2\mu}\frac{\partial^2}{\partial R^2} + V(R,\theta_n) - W_0(\theta_n)\right]\phi_0(R;\theta_n) = 0 \qquad (13)$$

and the N $\phi_0(R;\theta_n)$ functions are further orthogonalized through a Schmidt procedure, which leads to an orthonormal set of $\{f_n(R)\}_{n=1,N}$ functions.

Once the He$-$Cs$_2$ interaction is expanded into Legendre polynomials, and the quadratures over radial functions are evaluated numerically, all the necessary matrix elements of the Hamiltonian eq 7 involving angular functions of type eq 9 become analytical.[29,30] Depending on the size of the resulting matrix, the eigenvalue problem is then solved using standard routines[36] or iterative algorithms.[37]

B. Adiabatic Angular Approach. An additional way to assess the accuracy of the analytical PES consists in performing approximate calculations involving just the potential curves parametrized in the relative He$-$Cs$_2$ orientation. To this end, we resort to an earlier adiabatic angular model[29] which we used to describe the vibrational predissociation of triatomic van der Waals complexes. In this model, the Schrödinger equation associated to the Hamiltonian of eq 7

$$\hat{H}\Psi(R,\hat{r}) = \hat{E}\Psi(R,\hat{r}) \qquad (14)$$

is solved, for discrete states, assuming a factorization of the type

$$\Psi(R,\hat{r}) = \phi_v(R;\theta)\psi_m^{(v)}(\theta) \qquad (15)$$

where ϕ, which describes the vibration along the R coordinate, is a solution at each orientation θ of the 1D equation

$$\left[-\frac{\hbar^2}{2\mu}\frac{\partial^2}{\partial R^2} + V(R,\theta) - W_v(\theta)\right]\phi_v(R;\theta) = 0 \qquad (16)$$

which is nothing but eq 13 for $v = 0$. The eigenvalues $W_v(\theta)$ in eq 16 constitute an effective potential for the angular motion described by $\psi_m^{(v)}$,

$$\left[B_e\hat{j}^2 + \frac{\hat{l}^2}{2\mu\bar{R}^2} + W_v(\theta)\right]\psi_m^{(v)}(\theta) = E_m^{(v)}\psi_m^{(v)}(\theta) \quad (17)$$

where a suitable average distance $\bar{R}$ has been considered. A variational solution of eq 17 is fairly straightforward, once the $W_v(\theta)$ potentials are expanded in Legendre polynomials using

an angular basis set of type eq 12. The energies, E_m^v are then labeled by a vibrational quantum number v and a rotational quantum number m, corresponding to the bending motion. This treatment, in fact, involves an adiabatic approximation[29] that neglects the effect of the angular momentum operators on the vibrational wave function $\phi_v(R; \theta)$

$$k^2 \Psi(\mathbf{R}, \hat{\mathbf{r}}) \approx \phi_v(R;\theta) k^2 \psi_m^{(v)}(\theta), \quad k = j, \ell \quad (18)$$

and is justified for those systems in which the internal (relative) rotational motion is much slower than the vibrational motion along the R coordinate.

C. The Quantum Monte Carlo Treatment. The Quantum Monte Carlo approach which we employ here to calculate the lowest bound state is divided into two main steps: the optimization of the trial wave function Ψ_T through a minimization procedure implemented in a Variational Monte Carlo (VMC) code[38] and the use of Ψ_T to solve by a random walk the imaginary-time dependent Schrödinger equation in the importance sampling form

$$-\frac{\partial f(\mathbf{R}, \tau)}{\partial \tau} = -D\nabla^2 f(\mathbf{R}, \tau) + \nabla[\mathbf{F}_D(\mathbf{R}) f(\mathbf{R}, \tau)] + [E_L(\mathbf{R}) - E_T] f(\mathbf{R}, \tau) \quad (19)$$

where $\mathbf{F}_D(\mathbf{R})$ is the quantum force given by

$$\mathbf{F}_D(\mathbf{R}) = \nabla \ln|\Psi_T(\mathbf{R})|^2 \quad (20)$$

$E_L(\mathbf{R})$ is the local energy given by

$$E_L(\mathbf{R}) = \Psi_T(\mathbf{R})^{-1} \hat{H} \Psi_T(\mathbf{R}) \quad (21)$$

$D = 1/2 \mu$ with μ being the reduced mass of the complex and $f(\mathbf{R}, \tau) = \Psi(\mathbf{R}, \tau) \Psi_T(\mathbf{R})$ is the distribution function.

The trial wave function of the $Cs_2-^{3,4}He$ system takes into account the correct symmetry of an homonuclear molecule[39]

$$\ln[\Psi_T(R, \cos\theta)] = f_0^{Imp-He}(R)[P_0(\cos\theta) + 1] + \sum_{n=1}^{n_{max}} \{f_{2n}^{Imp-He}(R)[P_{2n}(\cos\theta) + 1] + f_{-2n}^{Imp-He}(R)[-P_{2n}(\cos\theta) + 1]\} \quad (22)$$

where f_v^{Imp-He} is a Jastrow correlation factor

$$f_v^{Imp-He}(R) = -\left(\frac{p_5}{R^5} + \frac{p_3}{R^3} + \frac{p_2}{R^2} + p_1 R + p_0 \ln R\right) \quad (23)$$

and P_v are the Legendre polynomials.

The Diffusion Monte Carlo (DMC) procedure relies on the short-time approximation[38] and the Schrödinger equation is solved iteratively in the integral form through a relaxation process in imaginary time

$$\Psi(\mathbf{R}', \tau_{k+1}) = \int G(\mathbf{R}' \leftarrow \mathbf{R}, \tau) \Psi(\mathbf{R}, \tau_k) d\mathbf{R} \quad (24)$$

where $\tau = \tau_{k+1} - \tau_k$ becomes now the discretized time step and the Green's function, given by

$$G(\mathbf{R}' \leftarrow \mathbf{R}, \tau) = \langle \mathbf{R}'|\exp(-\tau(\hat{H} - E_T))|\mathbf{R}\rangle \quad (25)$$

can be interpreted as the "transition" probability to move to a new position $\mathbf{R}'$ in the time step τ. The projection operator in eq 25 extracts the ground state wave function Ψ_0 from an arbitrarily chosen initial state, written as a linear combination of the eigenfunctions Ψ_i of $\hat{H}$, $\Psi_0 = \Sigma_i c_i \Psi_i$, when $\tau \to \infty$

$$\lim_{\tau\to\infty} \exp(-\tau(\hat{H} - E_T)) \sum_i c_i \Psi_i(\mathbf{R}) \Psi_T(\mathbf{R}) =$$
$$\lim_{\tau\to\infty} \sum_i \exp(-\tau(E_i - E_T)) c_i \Psi_i(\mathbf{R}) \Psi_T(\mathbf{R}) = \quad (26)$$
$$\exp(-\tau(E_0 - E_T)) c_0 \Psi_0(\mathbf{R}) \Psi_T(\mathbf{R})$$

The DMC ground state $f_0 = \Psi_0 \Psi_T$ is reached by simulating the imaginary-time diffusion of replicas (walkers) of the system in the configurational space. The Green's function is generally unknown; in the importance sampling DMC framework[38,40] the Green's function is splitted into two different contributions, according to the Trotter formula:

$$G(\mathbf{R}' \leftarrow \mathbf{R}, \tau) \simeq \tilde{G}(\mathbf{R}' \leftarrow \mathbf{R}, \tau) = G_d(\mathbf{R}' \leftarrow \mathbf{R}, \tau) \times$$
$$G_b(\mathbf{R}' \leftarrow \mathbf{R}, \tau) = (4\pi D\tau)^{-3/2} \times$$
$$\exp\left[-\frac{[\mathbf{R}' - \mathbf{R} - D\tau\mathbf{F}_D(\mathbf{R})]^2}{4D\tau}\right] \times$$
$$\exp\left\{\left[E_T - \frac{E_L(\mathbf{R}) + E_L(\mathbf{R}')}{2}\right]\tau\right\} \quad (27)$$

The

$$G_b = \exp\left\{\left[E_T - \frac{E_L(\mathbf{R}) + E_L(\mathbf{R}')}{2}\right]\tau\right\}$$

branching term can be considered as a rate term that rules the changes in the population of walkers.[38] From a "diffusional" point of view, this technique allows one to simulate the presence of "sources" and "sinks" in the imaginary time evolution of the process by replicating or "killing" the walkers. On average, walkers will die in regions where $\Psi_T > \Psi$ and give birth in regions where $\Psi_T < \Psi$. The branching scheme we have implemented is based on the algorithm presented in various earlier papers.[41,42] Each walker is characterized by a cumulative weight; at the j-th iteration the weight w_{ij} for the i-th walker is given by

$$w_{ij} = \prod_{k=1}^{j} b_{ik} \quad (28)$$

where

$$b_{ik} = \exp\left\{\left[E_T - \frac{E_L(\mathbf{R}_i) + E_L(\mathbf{R}'_i)}{2}\right]\tau\right\}$$

Structuring a Quantum Solvent around a Weakly Bound Dopant

J. Phys. Chem. A, Vol. 113, No. 52, 2009 **14725**
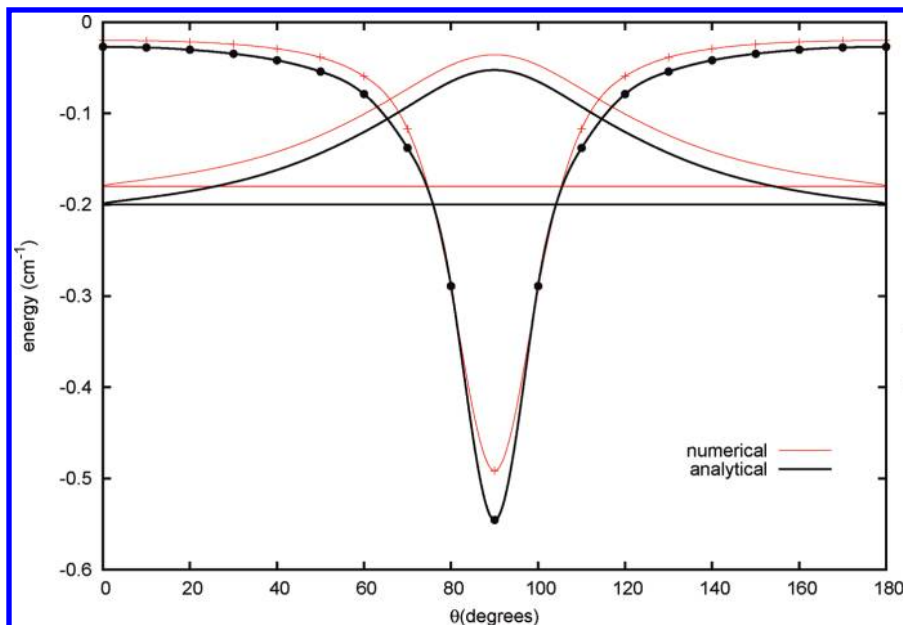

Figure 4. Effective potentials in the adiabatic approximation: light red lines, from numerical ab initio points; black lines, using the analytical fit. Also the corresponding angular distributions are depicted with respect to their bound state energies, see text.

The reference energy E_T is updated during the random walk, according to the following formula[43]

$$E_T = E_T + \frac{\alpha}{\tau} \ln \frac{N(\tau_{j-1})}{N(\tau_j)} \quad (29)$$

where α is a control parameter (to be chosen small) and $N(\tau_{j-1})$ and $N(\tau_j)$ represent the population of walkers in two successive steps of the random walk. Updating E_T is a fundamental tool to minimize the fluctuations in the ensemble. Walkers are killed or replicated by using two parameters w_{min} and w_{max} that allow for the following variable population of walkers:

• if $w_{ij} < w_{min}$, the i-th walker is destroyed with probability $p_- = 1 - w_{ij}$ and retained with probability $p_+ = w_{ij}$ and a weight equal to the average weight over the ensemble, $\bar{W}_j = \Sigma_i^N w_{ij}$;

• if $w_{ij} > w_{max}$, the i-th walker is replicated. The number of replicas is given by $N_w^{ij} = \text{int}(w_{ij} + \eta)$ where η is uniform random number $\in [0, 1]$. A new weight w_{ij}/N_w^{ij} is associated at these N_w^{ij} walkers;

• in the case $w_{min} \leq w_{ij} \leq w_{max}$, the i-th walker survives with no duplicates.

The average over the ensemble at the j-th iteration is

$$\langle \hat{O} \rangle_j = \frac{1}{W_j} \sum_{i=1}^{N} w_{ij} O_{i,j} \quad (30)$$

where $W_j = \Sigma_i^N w_{ij}$. The final estimate of the observable O is obtained by the usual definition of N_b blocks of M steps

$$\langle \hat{O} \rangle = \frac{\int \Psi_0(\mathbf{R}) \hat{O} \Psi_T(\mathbf{R}) d\mathbf{R}}{\int \Psi_0(\mathbf{R}) \Psi_T(\mathbf{R}) d\mathbf{R}} \simeq \frac{1}{N_b} \sum_{k=0}^{N_b-1} \left[\frac{1}{M} \sum_{j=k\times M+1}^{(k+1)\times M} \langle \hat{O} \rangle_j \right] \quad (31)$$

IV. Calculations and Results

A. Numerical Details. In the calculations presented here, the following masses (amu) were used: $m_{Cs} = 132.9054519$, $m_{^3He} = 3.0160374$, $m_{^4He} = 4.00260324$. The Cs_2 molecule was frozen at its equilibrium distance $r_{eq} = 6.8$ Å. A grid of 8192 points in the R range [2−200] Å was employed to solve numerically eq 13 using a Numerov procedure. The θ_n values were chosen as $\theta_n = [1 - (n-1)/(N-1)] \pi/2$, $n = 1, N$. To use the original ab initio points, the initial choice was of $N = 10$; this limit, however, was increased at will when using the analytical fit of the PES. To speed up the quadratures, an interpolation of 1000 Gaussian points in the above-mentioned R range was performed on the $\{f_n\}$ functions. The expansion of the He−Cs_2 analytical interaction in Legendre polynomials was done by considering 101 Gauss-Legendre points in the $[0, \pi]$ interval. To avoid spurious results, a cutoff of 5000 cm^{-1} was imposed on the interaction. At a total angular momentum $J = 0$ and inversion parity $\epsilon = +1$, energy convergence to within 10^{-3} cm^{-1} was achieved by using $N = 12$ and 10 even j values.

The DMC calculations have been carried out by using 2000 walkers; the imaginary-time simulation has been divided into 40 blocks of 60 000 time steps. The time step τ has been chosen to be equal to 300 for both sytems to achieve a 99.9% acceptance ratio during the random walk. For w_{min} and w_{max}, we have chosen 0.5 and 2.0, respectively; these values, together with $\alpha = 1.0$, allow us to stabilize the fluctuation of the population of the replicas.

B. Results. As mentioned above, an indirect way to assess the quality of the fit consists in applying the adiabatic angular approximation of Section IIIA to the original ab initio points, which now provides potential curves at 10 fixed orientations from 0 to 90° and also to the analytical potential at the same angular configurations. In both cases, and for all orientations, solving eq 16 leads to the presence of only one bound level. The corresponding angular adiabatic energies, $W_0(\theta)$, are depicted in Figure 4 and denoted as numerical (from ab initio points), and analytical, respectively. As can be realized from inspecting the figure, the results from the analytical surface overestimate the binding energy up to a maximum of ∼0.05

TABLE VI: Rotational (j) and Vibrational (n) Distributions of the Bound State Found at $J = 0$ for Each Helium Isotope[a]

j	$E_{^4\text{He}} = -0.106 \text{ cm}^{-1}$	$E_{^3\text{He}} = -0.042 \text{ cm}^{-1}$
0	$86.3401250378317 \times 10^{-2}$	$93.608592444636 \times 10^{-2}$
2	$12.3678351471421 \times 10^{-2}$	$5.87530060869408 \times 10^{-2}$
4	$1.15438376393513 \times 10^{-2}$	$4.54365148613764 \times 10^{-3}$
6	$1.21124084530109 \times 10^{-3}$	$5.27232367648316 \times 10^{-4}$
8	$1.41275979301269 \times 10^{-4}$	$7.26608831972656 \times 10^{-5}$
10	$1.99197836306531 \times 10^{-5}$	$1.38016512580359 \times 10^{-5}$
12	$3.39896073941494 \times 10^{-6}$	$3.05529630052595 \times 10^{-6}$
14	$6.01672832839106 \times 10^{-7}$	$5.70884529637803 \times 10^{-7}$
16	$1.09274554622377 \times 10^{-7}$	$8.76893608110321 \times 10^{-8}$
18	$1.39945502705227 \times 10^{-8}$	$9.20826920556535 \times 10^{-9}$

n	$E_{^4\text{He}} = -0.106 \text{ cm}^{-1}$	$E_{^3\text{He}} = -0.042 \text{ cm}^{-1}$
1	$58.4580298206451 \times 10^{-2}$	$46.8373534785016 \times 10^{-2}$
2	$34.1120748328049 \times 10^{-2}$	$39.4835985102445 \times 10^{-2}$
3	$6.99864483965479 \times 10^{-2}$	$12.1668950931790 \times 10^{-2}$
4	$2.76891022174691 \times 10^{-3}$	$1.10063966120214 \times 10^{-2}$
5	$7.02785084280033 \times 10^{-4}$	$1.09987803481179 \times 10^{-3}$
6	$3.29798897934088 \times 10^{-4}$	$7.99918768777823 \times 10^{-4}$
7	$2.16592307113333 \times 10^{-4}$	$6.51233704831959 \times 10^{-4}$
8	$1.63924965253360 \times 10^{-4}$	$1.03452865432662 \times 10^{-3}$
9	$8.97443573410788 \times 10^{-5}$	$3.86697189366526 \times 10^{-4}$
10	$3.18023063031115 \times 10^{-5}$	$1.22884656037730 \times 10^{-4}$
11	$8.07631156026722 \times 10^{-6}$	$1.89929871446577 \times 10^{-5}$
12	$8.70617420475831 \times 10^{-7}$	$9.98573429769180 \times 10^{-7}$

[a] They are of $\epsilon = +1$, $\eta = +1$ symmetry. The corresponding energies are included at the top.

cm^{-1} at 90°. After expansion of these effective potentials up to 10 (even) Legendre polynomials, the solution of the angular motion, eq 17, for $J = 0$, $\epsilon = +1$, $\eta = +1$, and $\bar{R} = 10$ Å, produces energies E_0^0 for the ^{4}He−Cs$_2$ complex of −0.1805 and −0.1988 cm^{-1}, respectively. Therefore, using the proposed analytical fit leads to a reduction of the overestimation of the binding energy by ∼0.02 cm^{-1}, which is in accord with the standard deviation already found before. The corresponding angular distributions, $|\psi_0^0(\theta)|^2$, are also depicted in Figure 4, and are seen to be nearly identical. They were plotted taking the origin of the vertical axis at their respective E_0^0 energies.

Using the analytical surface, additional variational calculations were carried out for helium−cesium dimer complexes containing either ^{4}He or ^{3}He. A single rotationless ($J = 0$) state of even inversion parity $\epsilon = +1$ and even interchange of cesium atoms $\eta = +1$ was found for the two species. Table VI collects the numerical characteristics of these states. In the bosonic case, the binding energy is roughly one-half of that predicted through the adiabatic approximation, a result which constitutes a lower limit to the binding energy. Inclusion of diagonal coupling terms, by relaxing conditions of eq 18, in order to also estimate the corresponding upper limit is presently outside the scope of our study. In relation with the distribution of rotational diatomic states, one finds that the $j = 0, 2$ states account for more than 98% of that distribution, which is a clear manifestation of the floppiness of this complex. In turn, the distribution of vibrational (n) states does not have a simple interpretation. In fact, n does not denote a quantum number and only labels the corresponding radial function coming from the orthogonalization procedure. Since we start from the ground level at $\theta = \pi/2$, $n = 1$ is the only unchanged function during the process. It accounts for almost 60% of the bound state showing the importance of the T-shaped arrangement for this system.

Concerning the fermionic scenario, the results appear to be chiefly a consequence of the lighter mass of the ^{3}He ($m_{^3\text{He}}/m_{^4\text{He}} \simeq 0.75$) partner. However, the binding energy of this complex
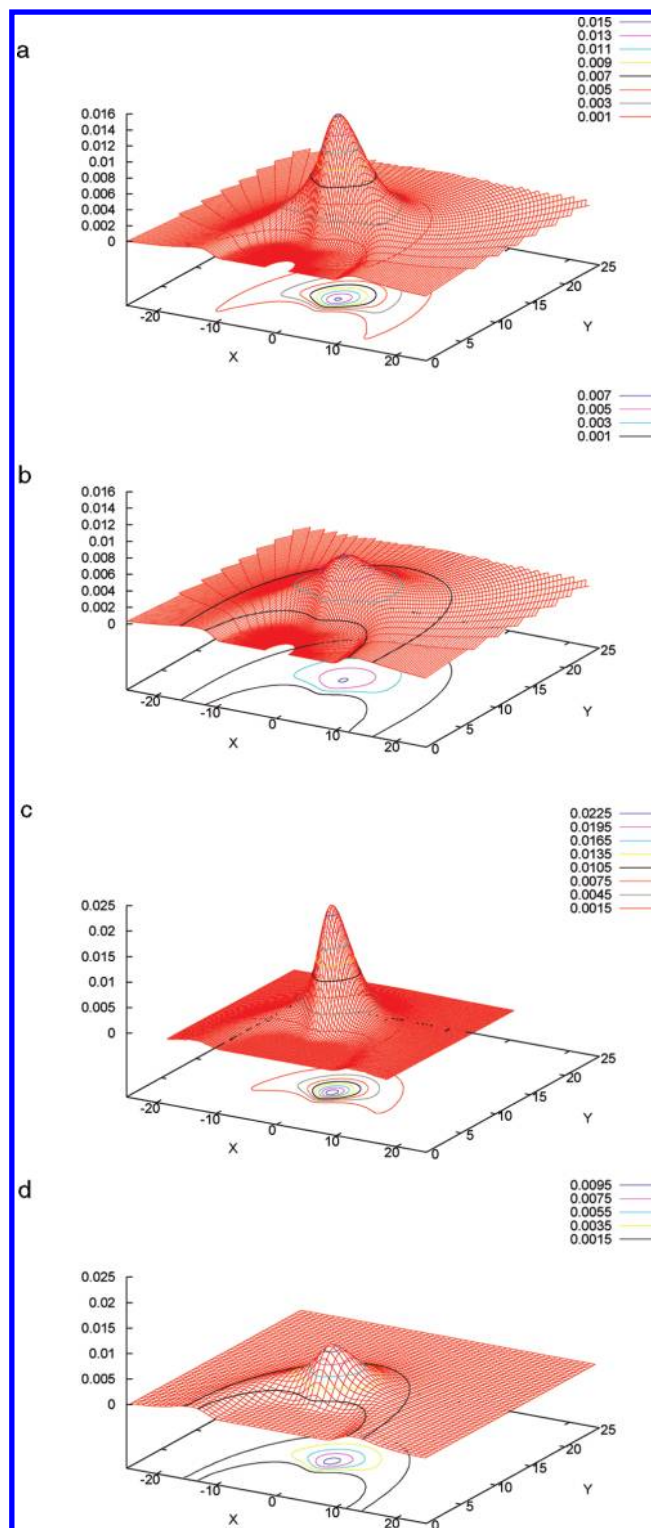

Figure 5. Probability density (Å^{-2}) of the He atom around the Cs$_2$ molecule in terms of $X = R \cos\theta$ and $Y = R \sin\theta$ distances (Å). Variational and DMC results for (a,c) ^{4}He, and (b,d) ^{3}He, respectively. The cesium atoms are placed at $(X,Y) = (\pm 3.4, 0)$.

is 40% lower than that containing ^{4}He. Because of the error presumably involved in the ab initio calculations plus that introduced by the present analytical fit, the presently predicted value of −0.04 cm^{-1} should be considered to be merely indicative of its expected, exact value. Again, the first two rotational diatomic states account for more than 99% of the distribution, suggesting that this complex is even more floppy
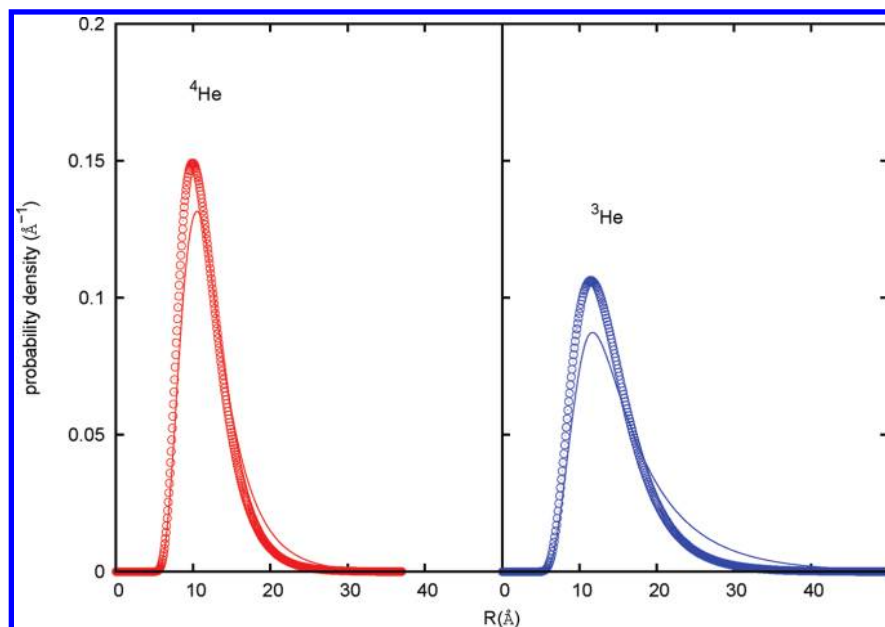
Structuring a Quantum Solvent around a Weakly Bound Dopant

J. Phys. Chem. A, Vol. 113, No. 52, 2009 **14727**

Figure 6. Radial distributions of boson (left panel) and fermion (right panel) partner in He−Cs$_2$ complexes from variational (solid lines) and DMC (circles) calculations.

than the bosonic one. The $n = 1$ radial state ($\theta = \pi/2$) is also dominant, although it accounts for less than 50% of the bound state.

It is interesting to note here how well the DMC final results on both systems agree with the variational calculations; the ground state energy for the ^{4}He−Cs$_2$ complex was found to be $-0.1072(9)$ cm^{-1}, while the corresponding value for the ^{3}He−Cs$_2$ complex was found to be $-0.0449(6)$ cm^{-1}. Clearly, both findings are very close to the variational calculations described before.

Figure 5a,b shows the probability densities of either the boson or fermion He atom, respectively, within the complex. They were obtained through variational calculations. The coordinates are $X = R \cos(\theta)$ and $Y = R \sin(\theta)$, and the contour plots are on the XY plane. We see that the ^{4}He (Figure 5a) is mainly located at the T-shaped orientation and at a distance of ∼10 Å from the dimer center of mass. However, it explores an ample region of the space which reaches distances larger than 20 Å, including almost linear arrangements. For the case of the ^{3}He (Figure 5b), the situation is similar; it shows some preference for being a T-shaped complex at R ∼10 Å, but the spatial spreading is much more evident and its bound wave function clearly populates linear configurations out to R ∼15 Å. The corresponding probability densities coming from the DMC calculations are given by Figure 5c,d. They are similar to the variational ones and essentially cover the same spatial region, but become less extended. This is in accord with the fact that the DMC binding energies result slightly higher than those coming from variational calculations. In particular, the density corresponding to ^{4}He (Figure 5c) shows a peak clearly more pronounced than the exhibited by the variational one (Figure 5a).

Figure 6 shows (DMC and variational) radial distributions of the distance of the bosonic (left panel) and fermionic (right panel) atoms from the cesium dimer center of mass. From both type of calculations, and as already seen in the previous figures, the two species show a maximum at R ∼10 Å, but the extension of the complexes is quite different as ^{4}He reaches up to ∼30 (∼25 from DMC) Å while ^{3}He shows a non-negligible presence at 40 (35 from DMC) Å and beyond. As discussed above, DMC distributions show higher peaks than their variational counterparts.

Figure 7 depicts the corresponding angular distributions in terms of cos(θ). For ^{4}He it is clear the preference for the T-shape arrangement, although the distribution explores linear configurations with a probability density of ∼10%. ^{3}He, in turn, prefers the perpendicular orientation but the linear ones account for almost 30% of the distribution, thus showing a remarkable increase of isotropy for its bound state. Both figures also report the same curves obtained from the DMC calculations and clearly confirm the good agreement between the results of the two methods.

To assess the relevance of the electronic spin of cesium dimer (triplet) in either getting or missing a bound triatomic level, we have performed additional variational calculations. To this end, replacing the spherical harmonics $Y_{j\Omega}(\theta, \phi)$ in the angular basis of eq 9 by $\mathscr{D}_{\Omega\Sigma}^{j*}(\phi, \theta, 0)$,[44] Σ being the common projection of $\hat{\boldsymbol{j}}$ and $\hat{\boldsymbol{S}}$ on $\boldsymbol{r}$, we consider the scenario in which only the diagonal elements of the $\hat{N}^2 = (\hat{\boldsymbol{j}} - \hat{\boldsymbol{S}})^2$ operator are accounted for. Inclusion of nondiagonal terms should lead to an increase the binding energy of ground triatomic levels. In practice, the approach reduces to replacing the $j(j + 1)$ terms in the Hamiltonian matrix by $j(j + 1) + S(S + 1) - 2\Sigma^2$. For a triplet state and for its least favored situation of $\Sigma = 0$, these terms become $j(j + 1) + 2$ and thus contribute to increasing the diatomic rotational energy with respect to the pseudo-$^1\Sigma$ calculations. As a consequence, in the boson (fermion) scenario, the $^1\Sigma$ binding energy decreases from -0.106 (-0.042) to -0.095 (-0.032) cm^{-1} in the $^3\Sigma$ framework, while the distributions of the corresponding states remain almost identical.

Finally, in order to evaluate the effect of fixing the cesium dimer's bond length, and within the above-mentioned $^3\Sigma$ approximation we have repeated variational calculations at $J = 0$ for different values of r; its variations indeed affect the diatomic rotational contribution to the energy and also the trimer interaction energy, a contribution that is automatically included through our analytical representation. Figure 8 displays for a broad range of interdiatomic distances the binding energies of the two species studied. At all the distances considered, the two triatomic systems are bound with the only exception being the case of the fermionic species, which at $r = 2$ Å becomes embedded into the continuum of the triatomic complex. Note that by adding all along these curves the overestimation coming
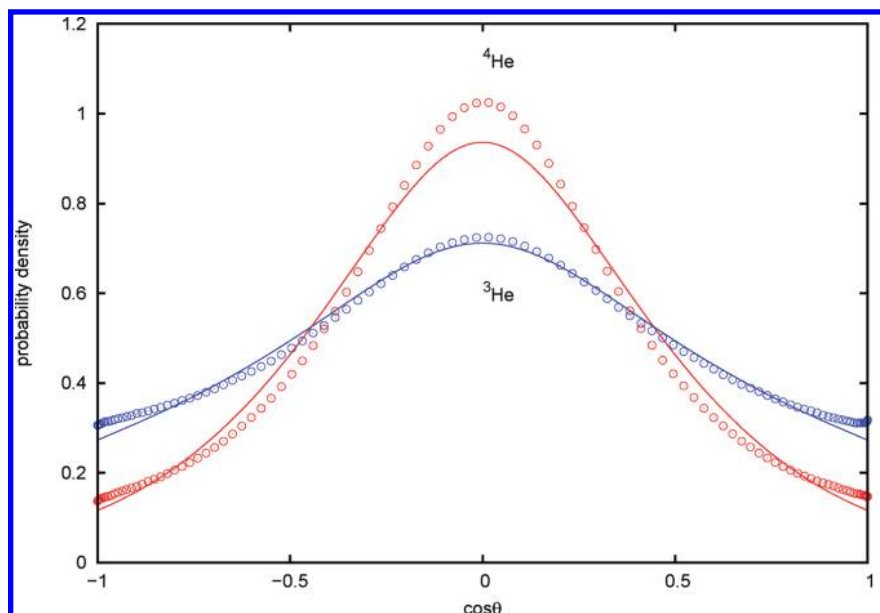
Figure 7. Angular distributions of boson and fermion partner in He—Cs_2 complexes from variational (solid lines) and DMC (circles) calculations.
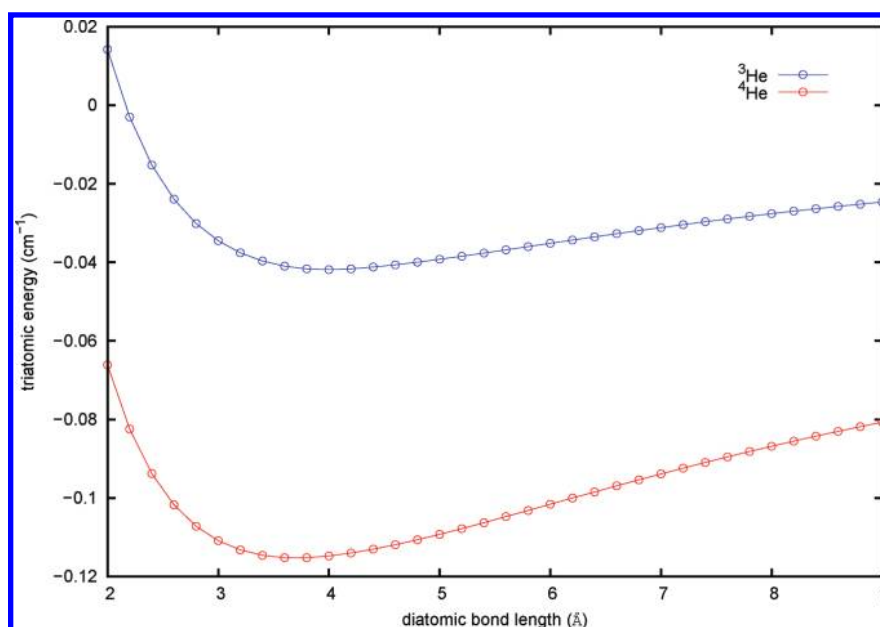

Figure 8. Triatomic energies of He—Cs_2 complexes as function of the r interdiatomic distance.

from the analytical fit, 0.02 cm^{-1}, the two systems indeed remain bound at the relevant interdiatomic distances.

V. Conclusions

In order to assess as accurately as possible the effects of the interaction forces on the existence and features of bound states for this apparently simple but very weakly bound complex, we have reported new CCSD(T) ab initio calculations of He—Cs_2 interaction with the molecular partner in its excited $^3\Sigma_u$ electronic state, freezing the cesium dimer structure at its equilibrium distance. For 10 different relative orientations from 0 to 90° at intervals of 10°, distances from helium to the center of mass of Cs_2 ranging from 2 to 20 Å were considered. Relativistic effects are included with the use of ECPs for Cs atoms, together with large correlation consistent basis sets.

We have implemented an analytic representation for the interaction potential of the HeCs$_2$($^3\Sigma$) complex. The new

functional form reproduces reasonably well all ab initio data with energies lower than 5 cm^{-1} with partial averaged deviations of ∼0.03 cm^{-1} (which reduces in fact to ∼0.02 cm^{-1} as shown through adiabatic angular dynamical calculations) therefore allowing us to carry out the study of the three-particle He—Cs_2 complex. This initial step is essential for the further analysis of larger complexes containing several helium atoms where it will be of interest to analyze the influence of the spin statistics of the solvent on the behavior of the cesium dimer within or outside the He droplet.[45]

We performed bound state calculations using two different methods, variational and Monte Carlo, as discussed in the previous sections. Computations for the two possible helium isotopes predict very small binding energies and large spatial spreading in both cases, although the fermionic complex results to be markedly more floppy than its bosonic counterpart. To assess the effect of the electronic spin of the cesium dimer and

the effect of fixing its bond length, additional variational calculations were carried out. The corresponding results show the robustness of all the approximations involved in the present study. Together with the ab initio data points, the final, analytic fit of the corresponding PES is made available to the scientific community. It will be employed in our group for further analysis of the structural properties of larger droplets of ^{3}He or superfluid ^{4}He.[10,46−53]

References and Notes

(1) Bloch, I.; Dalibard, J.; Zwenger, W. *Rev. Mod. Phys.* **2008**, *80*, 885.

(2) Monroe, C. *Nature* **2002**, *416*, 238.

(3) Doyle, J.; Friederich, B.; Krems, R. V.; Masnou-Seeuws, F. *Eur. Phys. J. D* **2004**, *31*, 149.

(4) Krems, R. V. *Phys. Chem. Chem. Phys.* **2008**, *10*, 4079.

(5) Bodo, E.; Gianturco, F. A.; Dalgarno, A. *J. Phys. B* **2002**, *35*, 2391.

(6) Weinstein, J. D.; de Carvalho, R.; Guillet, T.; Friederich, B.; Doyle, J. *Nature* **1998**, *395*, 148.

(7) Bakker, J. M.; Stoll, M.; Weise, D. R.; Vogelsong, O.; Meijer, G.; Peters, A. *J. Phys. B* **2006**, *39*, 51111.

(8) Morris, J. G. E.; Michniak, R. A.; Nguyen, S. V.; Campbell, W. C.; Egorov, D.; Maxwell, S. E.; van Burren, L. D.; Doyle, J. *Rev. Sci. Instrum.* **2004**, *75*, 17.

(9) Bodo, E.; Gianturco, F. A. *Int. Rev. Phys. Chem.* **2006**, *25*, 313.

(10) de Lara-Castells, M. P.; Prosmiti, R.; López-Durán, D.; Delgado-Barrio, G.; Villarreal, P.; Gianturco, F. A.; Jellinek, J. *Int. J. Quantum Chem.* **2007**, *107*, 2902.

(11) Jones, K. M. *Rev. Mod. Phys.* **2006**, *78*, 483.

(12) Durr, S.; Volz, T.; Marte, A.; Rempe, G. *Phys. Rev. Lett.* **2004**, *92*, 020406.

(13) Toennies, J. P.; Vilesov, A. F. *Angew. Chem., Int. Ed.* **2004**, *43*, 2622.

(14) Hartmann, M.; Miller, R. E.; Toennies, J. P.; Vilesov, A. F. *Science* **1996**, *272*, 1631.

(15) Farnik, M.; Toennies, J. P. *J. Chem. Phys.* **2005**, *122*, 014307.

(16) Ernst, W. E.; Huber, R.; Jiang, S.; Beuc, R.; Movre, M.; Pichler, G. *J. Chem. Phys.* **2006**, *124*, 024313.

(17) Frisch, M. J.; Trucks, G. W.; Schlegel, H. B.; Scuseria, G. E.; Robb, M. A.; Cheeseman, J. R.; Montgomery, Jr., J. A.; Vreven, T.; Kudin, K. N.; Burant, J. C.; Millam, J. M.; Iyengar, S. S.; Tomasi, J.; Barone, V.; Mennucci, B.; Cossi, M.; Scalmani, G.; Rega, N. G. A.; Petersson, G. A.; Nakatsuji, H.; Hada, M.; Ehara, M.; Toyota, K.; Fukuda, R.; Hasegawa, J.; Ishida, M.; Nakajima, T.; Honda, Y.; Kitao, O.; Nakai, H.; Klene, M.; Li, X.; Knox, J. E.; Hratchian, H. P.; Cross, J. B.; Adamo, C.; Jaramillo, J.; Gomperts, R.; Stratmann, R. E.; Yazyev, O.; Austin, A. J.; Cammi, R.; Pomelli, C.; Ochterski, J. W.; Ayala, P. Y.; Morokuma, K.; Voth, G. A.; Salvador, P.; Dannenberg, J. J.; Zakrzewski, V. G.; Dapprich, S.; Daniels, A. D.; Strain, M. C.; Farkas, O.; Malick, D. K.; Rabuck, A. D.; Raghavachari, K.; Foresman, J. B.; Ortiz, J. V.; Cui, Q.; Baboul, A. G.; Clifford, S.; Cioslowski, J.; Stefanov, B. B.; Liu, G.; Liashenko, A.; Piskorz, P.; Komaromi, I.; Martin, R. L.; Fox, D. J.; Keith, T.; Al-Laham, M. A.; Peng, C. Y.; Nanayakkara, A.; Challacombe, M.; Gill, P. M. W.; Johnson, B.; Chen, W.; Wong, M. W.; Gonzalez, C.; Pople, J. A. *Gaussian03*, Revision B.05;Gaussian, Inc.: Pittsburgh, PA, 2003.

(18) Hay, P. J.; Wadt, W. R. *J. Chem. Phys.* **1985**, *82*, 299.

(19) Leininger, T.; Nicklass, A.; Küchle, W.; Stoll, H.; Dolg, M.; Bergner, A. *Chem. Phys. Lett.* **1996**, *255*, 274.

(20) Lim, I. S.; Schwerdtfeger, P.; Metz, B.; Stoll, H. *J. Chem. Phys.* **2005**, *122*, 104103.

(21) Ross, R. B.; Powers, J. M.; Atashroo, T.; Ermler, W. C.; LaJohn, L. A.; Christiansen, P. A. *J. Chem. Phys.* **1990**, *93*, 6654.

(22) Xie, F.; Sovkov, V. B.; Lyyra, A. M.; Li, D.; Ingram, S.; Bai, J.; Ivanov, V. S.; Magnier, S.; Li, L. *J. Chem. Phys.* **2009**, *130*, 051102.

(23) Foucrault, M.; Millie, Ph.; Daudey, J. P. *J. Chem. Phys.* **1992**, *96*, 1257.

(24) Li, D.; Xie, F.; Li, L.; Magnier, S.; Sovkov, V. B.; Ivanov, V. S. *Chem. Phys. Lett.* **2007**, *441*, 39.

(25) Boys, S. F.; Bernardi, F. *Mol. Phys.* **1970**, *19*, 553.

(26) García-Gutierrez, L.; Delgado-Téllez, L.; Valdés, A.; Prosmiti, R.; Villarreal, P.; Delgado-Barrio, G. *J. Phys. Chem. A* **2009**, *113*, 5754.

(27) Pirani, F.; Brizi, S.; Roncaratti, L. F.; Casavecchia, P.; Cappelletti, D.; Vecchiocattivi, F. *Phys. Chem. Chem. Phys.* **2008**, *10*, 5489.

(28) Wernli, M.; Bodo, E.; Gianturco, F. A. *Eur. Phys. J. D* **2007**, *45*, 267.

(29) Beswick, J. A.; Delgado-Barrio, G. *J. Chem. Phys.* **1980**, *73*, 3653.

(30) Gianturco, F. A. *The transfer of molecular energy by collisions*; Springer: Berlin, 1979.

(31) Auböck, G.; Nagl, J.; Callegari, C.; Ernst, W. E. *J. Phys. Chem. A* **2007**, *111*, 7404.

(32) Lefebvre-Brion, H.; Field, R. W. *Perturbations in the Spectra of Diatomic Molecules*; Academic Press, Inc.: Orlando, FL, 1986.

(33) Aquilanti, V.; Cavalli, S.; Grossi, G. *Z. Phys. D* **1996**, *36*, 215.

(34) Secrest, D.; Eastes, W. *J. Chem. Phys.* **1972**, *56*, 2502.

(35) Roncero, O.; de Lara-Castells, M. P.; Delgado-Barrio, G.; Villarreal, P.; Stoecklin, T.; Voronin, A.; Rayez, J. C. *J. Chem. Phys.* **2008**, *128*, 164313.

(36) (a) Linear Algebra Package 3.2.1, 2009, http://www.netlib.org/lapack/. (b) Intel MKL 10.2, 2009, http://software.intel.com/en-us/intel-mkl/.

(37) Márquez-Mijares, M.; Pérez, de; Tudela, R.; González-Lezana, T.; Roncero, O.; Miret-Artés, S.; Delgado-Barrio, G.; Villarreal, P.; Baccarelli, I.; Gianturco, F. A.; Rubayo-Soneira, J. *J. Chem. Phys.* **2009**, *130*, 154301.

(38) Hammond, B. L.; Lester, W. A., Jr.; Reynolds, P. J. *Monte Carlo methods in ab initio quantum chemistry*; World Scientific: NJ, 1994.

(39) Bodo, E.; Coccia, E.; López-Durán, D.; Gianturco, F. A. *Phys. Scr.* **2007**, *76*, C104.

(40) Reynolds, P. J.; Ceperley, D. M.; Alder, B. J.; Lester, W. A., Jr. *J. Chem. Phys.* **1982**, *77*, 5593.

(41) Paesani, F.; Gianturco, F. A. *J. Chem. Phys.* **2002**, *116*, 10170.

(42) Paesani, F.; Gianturco, F. A. *J. Chem. Phys.* **2002**, *117*, 709.

(43) Viel, A.; Patel, M. V.; Niyaz, P.; Whaley, K. B. *Comput. Phys. Commun.* **2002**, *145*, 24.

(44) Roncero, O.; Buchachenko, A. A.; Lepetit, B. *J. Chem. Phys.* **2005**, *122*, 034303.

(45) Bovino, S.; Coccia, E.; Bodo, E.; López-Durán, D.; Gianturco, F. A. *J. Chem. Phys.* **2009**, *130*, 224903.

(46) López-Durán, D.; de Lara-Castells, M. P.; Delgado-Barrio, G.; Villarreal, P.; Di Paola, C.; Gianturco, F. A.; Jellinek, J. *Phys. Rev. Lett.* **2004**, *93*, 053401.

(47) López-Durán, D.; de Lara-Castells, M. P.; Delgado-Barrio, G.; Villarreal, P.; Di Paola, C.; Gianturco, F. A.; Jellinek, J. *J. Chem. Phys.* **2004**, *121*, 2975.

(48) de Lara-Castells, M. P.; López-Durán, D.; Delgado-Barrio, G.; Villarreal, P.; Di Paola, C.; Gianturco, F. A.; Jellinek, J. *Phys. Rev. A* **2005**, *71*, 033203.

(49) Di Paola, C.; Gianturco, F. A.; López-Durán, D.; de Lara- Castells, M. P.; Delgado-Barrio, G.; Villarreal, P.; Jellinek, J. *ChemPhysChem* **2005**, *6*, 1348.

(50) de Lara-Castells, M. P.; Prosmiti, R.; Delgado-Barrio, G.; López-Durán, D.; Villarreal, P.; Gianturco, F. A.; Jellinek, J. *Phys. Rev. A* **2006**, *74*, 053201.

(51) de Lara-Castells, M. P.; Prosmiti, R.; Delgado-Barrio, G.; Villarreal, P.; Mitrushchenkov, A. O. *J. Chem. Phys.* **2006**, *125*, 221101.

(52) de Lara-Castells, M. P.; Prosmiti, R.; López-Durán, D.; Delgado-Barrio, G.; Villarreal, P.; Gianturco, F. A.; Jellinek, J. *Phys. Scr.* **2007**, *76*, C96.

(53) de Lara-Castells, M. P.; Mitrushchenkov, A. O.; Delgado-Barrio, G.; Villarreal, P. *Few-Body Syst.* **2009**, *45*, 233.